

Understanding Nano-Impact Current Spikes: Electrochemical Doping of Impacting Nanoparticles

Enno Kätelhön, Ann Feng, Wei Cheng, Shaltiel Eloul, Christopher
Batchelor-McAuley, and Richard G. Compton*

*Department of Chemistry, Physical and Theoretical Chemistry Laboratory, Oxford
University, South Parks Road, Oxford, OX1 3QZ, United Kingdom*

E-mail: richard.compton@chem.ox.ac.uk

Phone: +44(0) 1865 275957

Abstract

We demonstrate the generic value of a rigorous analysis of spike shapes observed in nano-impact experiments. To this end, we investigate the electrochemical doping of insoluble nanoparticles impacting on a biased electrode surface and develop an analytical model of the doping process is developed that accounts for the diffusion of ions inside nanoparticles as well as a numerical model for the response characteristics of the analogue measurement circuitry. By this means, spike shapes that are experimentally observed in the electrode current are predicted and directly compared with experimental data, while appropriate fitting procedures allow detailed physical insights into the ionic mass transport within the particle. Using the oxidative doping of ferrocene nanoparticles with tetrafluoroborate anions as a paradigm case, we demonstrate that size distributions of particle populations showing excellent agreement with scanning electron microscopy measurements can be extracted from experimental data and ionic diffusion inside the particle can be quantified.

Introduction

Recent decades saw an ever growing interest in the fascinating properties of nanoparticles alongside a fast development in related scientific disciplines. In spite of these research efforts and the large number of studies being published, some central challenges still remain unsolved. These challenges include the development of an understanding of the toxicity of nano-scaled objects to humans that is still under controversial discussion while fast and cost-efficient detection methods remain relatively absent.

An upcoming technology that addresses the lack of detection methods is the nano-impact method,¹⁻⁴ which aims to provide cheap and widely-available tools for the electrochemical detection of nanoparticles. In this approach, an electrode is immersed into a solution containing freely diffusing nanoparticles, which by virtue of their Brownian motion may diffusively impact on the electrode surface. Once an electrical contact is established with the electrode

particles may enable a charge transfer due to either a catalytic reaction with the surrounding solution or their intrinsic electrochemical properties. The charge transfer can then be observed in the electrode current and may provide insight into the particle size distribution, if the overall transferred charge is often directly proportional to the particle volume. Populations of metallic⁵ or organic⁶ nanoparticles that dissolve upon impact on the electrode surface can for instance be seized via the integration of individual spikes.

Recently, Feng *et al.*⁷ reported the observation of electrochemical doping processes in nano-impact experiments. It was shown that anions are incorporated into the particle during the electrochemical oxidation of ferrocene nanoparticles in an aqueous solution containing sodium tetrafluoroborate. Herein, a tetrafluoroborate anion is taken up by the nanoparticle for each ferrocene molecule being oxidised and the particle is entirely oxidised if the electrode is set to a sufficiently high overpotential. Spikes can hence be used to determine the size of the impacting particles via the integration of individual spikes as demonstrated in the respective study⁷ and as elaborated in detail below.

While the frequency of nano-impacts and the charge transferred per impact are commonly used in the analysis of nano-impacts, other measured quantities are rarely discussed. Aside from the absence of appropriate analytical models in many cases, the reasons for this are twofold. First, unlike in other research disciplines such as neurophysiology, appropriate spike analysis software that is suitable for the analysis and fitting of large data sets is not available and, second, the fitting of analytical models to experimental data is often vastly complicated by the current response characteristics of the measurement devices that were used to record the investigated experimental data. When measuring low currents with standard potentiostats, data usually passes a low-pass filter, which may drastically alter the spike shape, if the bandwidth of the measurement is not sufficiently high.⁸ Even if filters can be bypassed and the potentiostat sampling rate is adequately high, the bandwidth will be limited by parasitic capacitances at the electrode, cables, connector or similar, so that knowledge and consideration of the potentiostat's transfer function are generally crucial.

Nevertheless, several studies focussing on the shape of impact spikes or individual features other than the spike integral can be found in literature. These studies include the discussion of spike shapes or features that arise from dissolving particles,^{8,9} surface charge diffusion on impacting particles,¹⁰ impacting liposomes¹¹ or emulsion droplets,¹² and enzymes¹³ to just name a few.

In this work, we demonstrate the generic value of the analysis of spike shapes in nano-impacts experiments. To this end, we first introduce an analytical model for the ionic doping of nanoparticles impacting on an electrode and derive an expression for time-dependency of the charge transfer at the electrode. This result is combined with a numerical model for the current response characteristics of a potentiostat, hence enabling the prediction of experimental spike shapes, and fitted to experimental data for the doping of ferrocene nanoparticles with tetrafluoroborate anions. By combining the theoretical knowledge of the doping process with experimental data, we demonstrate the benefit of an investigation of the recorded spike shapes: Solely on the basis of a spike shape analysis, size distributions of nanoparticle populations can be found showing an excellent agreement with scanning electron microscopy measurements. In addition, detailed physical insights into the ionic diffusion *inside* nanoparticles are enabled allowing a quantification of the mass transport inside the nanoparticle.

Theory

This section presents the derivation of a theoretical model for the electrochemical doping of nanoparticles through the diffusion of ions into the particle. We introduce the investigated theoretical model and provide the analytical solution for the spike shape of the electrode current.

Theoretical model

We model the diffusion of ions within a spherical particle of radius r_0 that initially is entirely depleted of the diffusing species. The number concentration c of the ions at the time $t = 0$ is hence given by:

$$c(\vec{r}, t = 0) = \begin{cases} 0 & \text{for } r < r_0 \\ c^* & \text{for } r = r_0 \end{cases} \quad (1)$$

where r is radial coordinate in spherical coordinates representing the distance from the particle centre. We further assume the ion concentration at the particle surface to be constant featuring a value of c^* at any time:

$$c(\vec{r}, t) = c^* \text{ for } r = r_0 \quad (2)$$

This assumption can be understood by considering the following two approximations: Firstly, since the diffusion of ions in the liquid outside the particle is much greater than in the solid inside and ions adsorb and enter the particle rapidly, the availability of ions at the particle surface is unlimited on the time scale of the diffusion inside the particle, if their inclusion into the particle is thermodynamically favourable. The ‘outside’ is hence not depleted of ions and diffusion on the ‘inside’ is rate determining with respect to the uptake of ions by the particle. The surface concentration of ions can hence be approximated to equal their solubility concentration in the particle at any time. Secondly, surface diffusion at the liquid-solid interface is assumed much faster than diffusion inside the particle, so we can consider the problem to be angular independent.

We further approximate the overall volume occupied by the ions taken up by the particle to be small in comparison to the particle volume so that the particle radius can be modelled to remain constant during the doping process. An illustration of the theoretical model can be found in Figure 1.

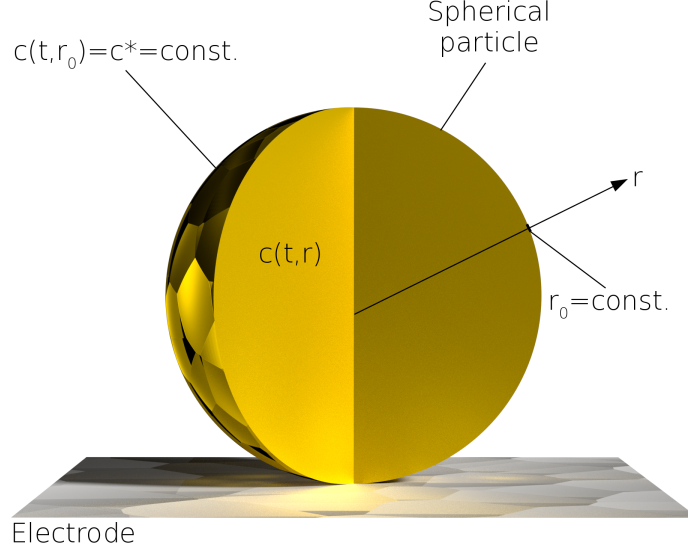


Figure 1: Illustration of the theoretical model employed for the diffusion of ions into the particle.

Due to the spherical symmetry of both the geometry and the boundary conditions, there cannot be any flux at centre of the particle and the concentration gradient at $r = 0$ must vanish at any time:

$$\left. \frac{\partial c(\vec{r}, t)}{\partial r} \right|_{r=0} = 0 \quad (3)$$

The diffusion of ions inside the sphere follows the diffusion equation $\partial_t c = D \Delta c$, where D is the diffusion coefficient of the considered species. Since all boundary conditions are symmetrical with respect to the particle centre, we may neglect the dependency of the Laplace operator on the solid angle, if it is expressed in spherical coordinates and if the origin of the coordinate system is set to the particle centre. The diffusion equation then simplifies to:

$$\frac{\partial c(r, t)}{\partial t} = D \left(\frac{\partial^2 c(r, t)}{\partial r^2} + \frac{2}{r} \frac{\partial c(r, t)}{\partial r} \right) \quad (4)$$

where we express c as a function of only one spatial dimension r rather than \vec{r} .

In the case of the electrochemical doping of ferrocene nanoparticles, we assume c^* equals the concentration of ferrocene inside the particle as for each one-electron-transfer reaction of a ferrocene molecule one ion is taken up by the particle. If the particle is located in the proximity of an appropriately biased electrode, where a net charge transfer between the electrode and the particle due to the electric field is facilitated and electro-neutrality of the particle must be conserved, the oxidation of ferrocene is hence assumed to be controlled by the diffusion of anions within the particle. In the case of a rapid charge transfer between the electrode and the particle so that c only depends on r and t , the total flux of charge I_{anal} into the particle as a function of time is given by:

$$I_{anal}(t) = -\frac{d}{dt} \int_{r < r_0} dV q_0 c(\vec{r}, t) \quad (5)$$

where q_0 is the charge of one ion. Assuming that the overall charge of the particle remains constant during the diffusion process, this current equals the current measured at an electrode that is located within tunnelling distance and that may exchange electrons with the particle.

The suggested model can be solved analytically as discussed in ‘Supporting Material A: Analytical’.^{14,15} A solution to the electrode current as a function of time is given by:

$$I_{anal}(t) = -8\pi c^* D q_0 r_0 \sum_{n=1}^{\infty} e^{-D\lambda_n^2 t} \quad (6)$$

and plotted for various diffusion coefficients in Figure 2.

Experimental

Particle synthesis and electrochemical measurements

Our analysis is based on published data,⁷ in which the oxidative doping of ferrocene nanoparticles was initially introduced and experimental details were provided in detail. In short,

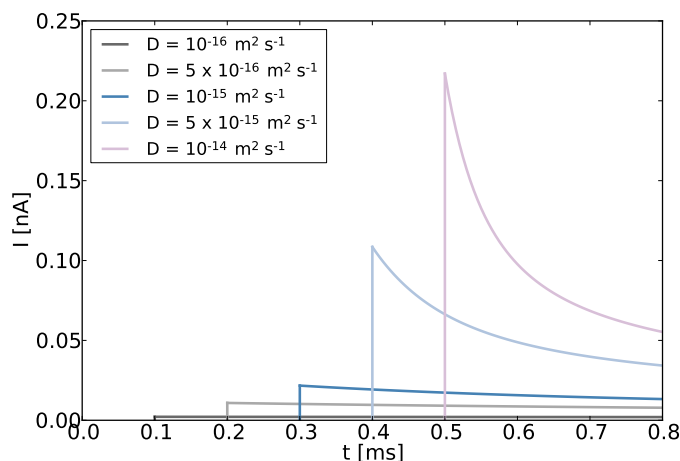


Figure 2: Spike shapes at varied diffusion coefficients. We evaluate the currents for a particle of the radius $r_0 = 50$ nm, a boundary concentration of $c^* = 3.6 \times 10^{27} \text{ mol}^{-1}$, and a number q of -1.602×10^{-19} C for the number of transferred elementary charges per ion. Data is calculated at a sampling frequency of 200 kHz and the first 30 terms of the sum are evaluated for the plot.

nanoparticles were synthesised via a re-precipitation method, in which ferrocene is first dissolved in acetonitrile, before the so-obtained solution is mixed with de-ionised water in a drop-wise fashion. During the mixing process the solution is vigorously stirred and subsequently sonicated. Nanoparticles were characterised via dynamic light scattering (DLS) and scanning electron microscopy (SEM), which exhibited good agreement, and were found to feature an average diameter of 104.6 ± 49.9 nm in the SEM measurement. Chronoamperograms were performed in 0.1 M sodium tetrafluoroborate using a carbon microdisk electrode featuring a diameter of $11 \mu\text{m}$.

Characterisation of the potentiostat

In order to determine any influence of the electronic circuitry and analogue-digital conversion of the employed potentiostat (Metrohm microAutolab Type II) on the measured signal, we experimentally determined the impulse response of the potentiostat to ensure that the overall amount of charge is conserved even if measured signals exceed the bandwidth of the potentiostat and for the later development of a related numerical model for our simulations.

A description of the related measurements can be found in the ‘Supporting Material B: Experimental’.

Analysis of experimental data

The section on computational methods is structured in three main parts. We first illustrate how the transfer function of the potentiostat is extracted from the recorded data and transferred into a computational model of the potentiostat’s current response. We then describe the automated spike-analysis and spike-fitting software that was developed for purpose of this study followed by a third section providing the physical parameters that employed in our calculations. Finite difference simulations used to verify the analytical model are discussed in the ‘Supporting Material C: Computational’ in the section ‘Finite-differences simulations’.^{16–18}

Modelling the current response characteristics of the potentiostat

On the basis of the impulse response measurements, we determine the transfer function of the potentiostat providing an exact description of how the potentiostat’s input signal is altered during the processing within its analogue circuitry and analogue-digital converter. To this end, we compare the measured impulse response with the impulse response of a first-order low-pass filter and find that both responses match well for a cutoff frequency of 48.0 Hz. Using this result, we develop a computational model of the filter via conformal mapping of the transfer function into time-discrete z-space and subsequent bilinear transformation. By this means, we obtain a computational model that predicts the response of the potentiostat to any input signal and enables us to model the experimentally-measured response to the current transient we found via the analytical model above. More detailed information on the filter modelling is provided in the ‘Supporting Material C: Computational’ in the section ‘Computational model of the filter response’.⁸

Automated spike analysis and fitting of the analytical model

For the purpose of this study, we developed an automated spike analysis-, integration-, and fitting software in *Python* and *C++*. Following an initial baseline subtraction, this software identifies spikes and fits the theoretical model of the current spikes to experimental data, while considering the potentiostat’s transfer function. By this means, we extract the particle radius r_0 and the ionic diffusion coefficient D within the particle solely from the measured spike shapes. A detailed discussion of the employed methods can be found in the ‘Supporting Material C: Computational’ in the sections ‘Automated spike finding’ and ‘Automated spike fitting’.

Physiochemical simulation parameters

In all calculations, we use fixed values for the density of ferrocene and its molar mass, which are set to $\rho = 1.11 \times 10^6 \text{ g m}^{-3}$ and $M = 186.04 \text{ g mol}^{-1}$ in accordance with the previous study.⁷ This leads to a boundary or saturation number concentration of $c^* = N_A \rho M^{-1} = 3.593 \times 10^{27} \text{ mol}^{-1}$. Furthermore, the charge transferred from the electrode to the particle per ion entering the particle is always set to $-e_0$ i.e. $q_0 = -1.602 \times 10^{-19} \text{ C}$ as discussed in the definition of the theoretical model.

Results and discussion

This section is divided into two parts focussing on the potentiostat’s current response characteristics and the physical insights that can be gained from the analysis of measured spike shapes, respectively. We first describe how the analytically-found spike shape, i.e. the predicted time-dependency of the charge transfer at the electrode surface, is altered by the potentiostat, before we then use our spike analysis software to demonstrate that the particle size distribution and the diffusion coefficient of ions inside nanoparticles can be determined solely through the analysis of spike shapes in combination with the theoretical model pre-

sented. Additionally, a numerical validation of the theoretical model via finite-differences calculations and a discussion of the numerical accuracy of our method is given in the ‘Supporting Material D: Numerical’.

Filter response to the analytical solution

In the above characterisation of the potentiostat, we found that the transfer function relating the charge transfer at the electrode and the eventually-measured current of the potentiostat can be modelled well as a first order low-pass filter operated at a cutoff frequency of 48 Hz. In order to compare experimental data with the analytical model, we therefore include the changes that the potentiostat imposes on the measured current in our model.

Using the previously-discussed implementations of the potentiostats transfer function, we determine the potentiostat response to the predicted charge transfer at the electrode shown above in Figure 2 and plot the resulting spikes in Figure 3. The comparison between the two figures reveals a drastic alteration of the initial solution. While the analytically calculated spikes only feature a length of few hundred microseconds, the transformed spikes exhibit significantly longer current transients of the order of hundreds of milliseconds. The inclusion of the potentiostat’s filter characteristics into the analytical model is hence a crucial requirement for the further analysis of the data.

The application of the low-pass filter may however mask high-bandwidth features of the input signal. Though the overall charge transferred is conserved, the potentiostat’s response to different input impulses may be identical if the bandwidth of the input signal is sufficiently high. In this case features of the initial signal may be entirely masked by the filter’s impulse response, which prohibits any further analysis of the spike with respect to parameters other than the overall transferred charge. We therefore investigate the potentiostat response to our analytical model of the charge transfer at the electrode using the parameter ranges that we employ in the fitting algorithm below and compare the potentiostat output signal with the predicted impulse response. The respective data can be seen in Figure 4 a) and b) for particles

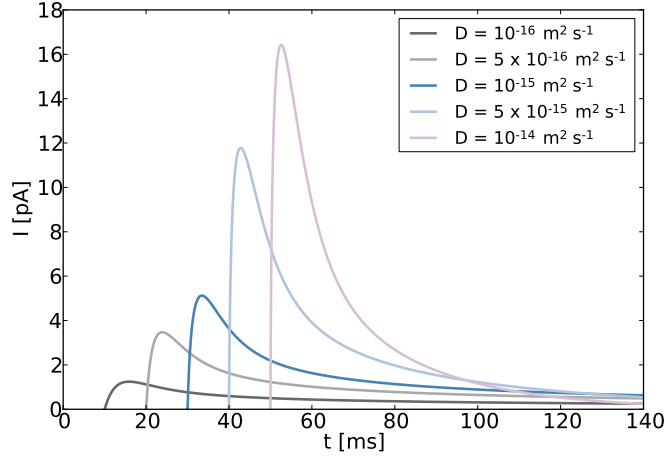


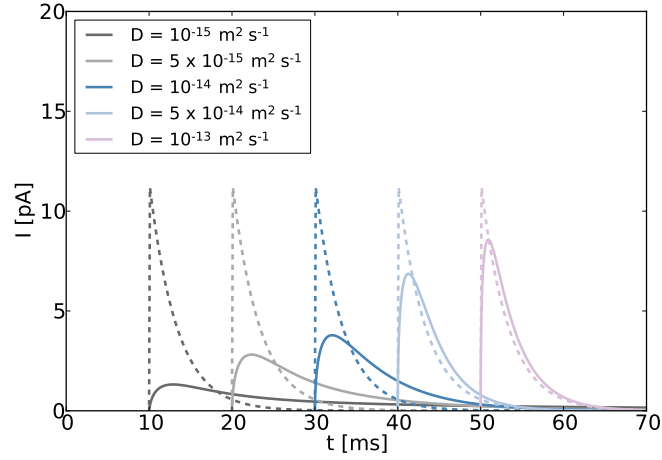
Figure 3: Analytical solutions for the current spikes shown in Figure 2 after the application of the filter model. Please note that for clarity spikes are separated by 10 ms rather than 100 μ s in the above figure. No oversampling is used when modelling the potentiostat’s transfer function.

of the radii 25 and 50 nm. In the plot, we can find that the modelled current transients for the electrochemical doping process converge towards the filters impulse response with increasing diffusion coefficients and decreasing particle radii, while the combination of a radius of 25 nm and a diffusion coefficient of $10^{-13} \text{ m}^2 \text{ s}^{-1}$ resembles the shape of the impulse response most-closely. It can however be seen that the influence of both the particle radius and the diffusion coefficient are well represented in the shape of the transformed spike though features are partly masked.

Comparison between theory and experiment

Following the analysis of the potentiostat’s transfer function, we employ our software algorithms to compare experimental data with the spike model presented by fitting the model through a least-squares approach. To this end, we first baseline-subtract experimental data and join all current measurements into a single time-current file, before we apply the spike detection algorithm to identify all measured spikes and to determine their exact peak positions. Next we use the spike fitting algorithm to fit our model individually to each spike

a)



b)

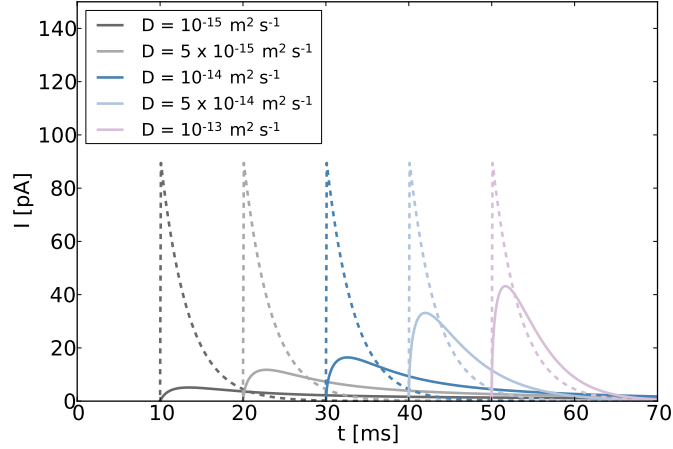


Figure 4: Comparison between the filtered analytical solution for the current transient as it would be measured by the potentiostat (solid lines) and the filter's impulse response (dashed lines) to a pulse featuring a length of $100 \mu\text{s}$ and an identical integral. a) and b) show the calculations for particles featuring radii of 25 and 50 nm, respectively. The data was calculated for a sampling frequency of 200 kHz and no oversampling was used to calculate the filter response.

detected in the experimental data. Several examples of such fits can be found in Figure 5 a) to c). In the plots we observe a good agreement between the experimental data and the spike model, which supports the applicability of the suggested model to the electrochemical doping of ferrocene nanoparticles. Within the limitations that are imposed on the fit by the current noise in the experiment, data can be fitted satisfactorily though individual features

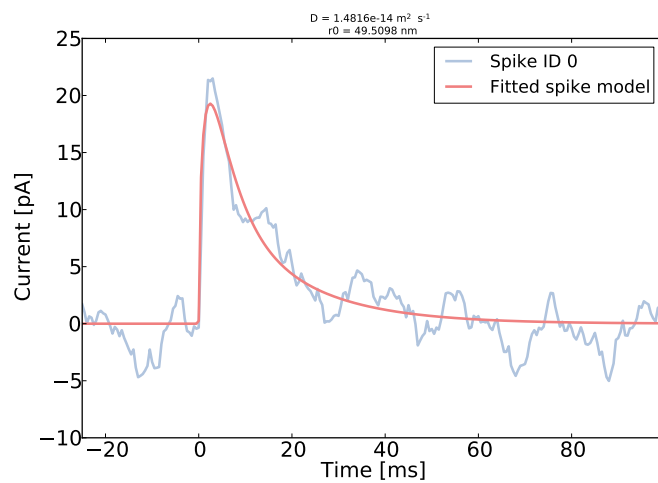
of the experimentally-found spikes cannot be directly compared with the spike model.

A more detailed insight can be achieved via a statistical analysis of the spike fitting results based on all fitted spikes. To this end, we plot the distributions of particle sizes in the Figure 6 a) in comparison with former scanning electron microscopy measurements⁷ that investigated the same particle population. We find that the average radius of the particle population is 42.7 ± 11.3 nm compared to 52.3 ± 25.0 nm in the previous study,⁷ the histograms show however very similar distributions. Given the fact that the experimental measurement is affected by current noise and that three parameters are fitted, we find thus a satisfactory agreement between the fit of our spike model and the experimental determination of the particle population's size distribution, which further supports the suggested diffusion mechanism. Aside from the current noise we attribute the deviation to two main effects: First, the baseline subtraction via a higher-order pronominal fit generally leads to an small overestimation of the baseline level in the proximity of the spikes, leading to a lowered spike integral and, hence, to a smaller particle radius in the analysis. Second, the baseline fit cannot account for the asymptotic spike tail, which is automatically removed from the analysis. Due to the noise level of the experimental data we however believe this effect to be only small. Figure 6 b) shows the distribution of diffusion coefficients that is obtained from the fit. Here we observe a unimodal distribution featuring an average diffusion coefficient of $(1.02 \pm 0.70) \times 10^{-14} \text{ m}^2 \text{ s}^{-1}$. As, to the best of our knowledge, diffusion coefficients during ionic doping processes of nanoparticles have never been reported before, we can however not compare this value with literature values.

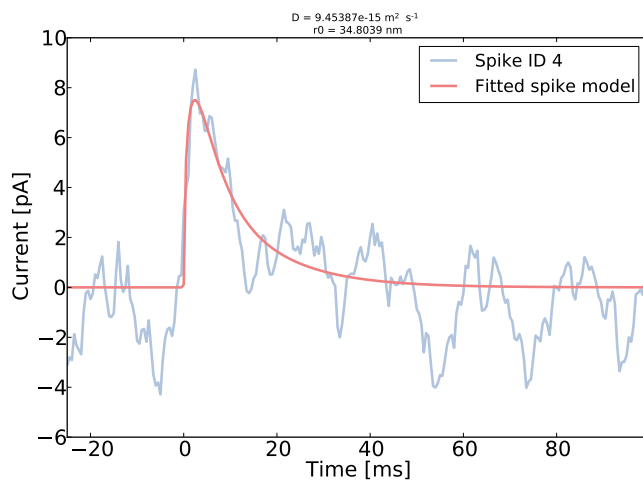
Conclusions

We demonstrate the generic value of spike shapes in nano-impact experiments, which in combination with appropriate theoretical models may reveal important additional information on the investigated system beyond.

a)



b)



c)

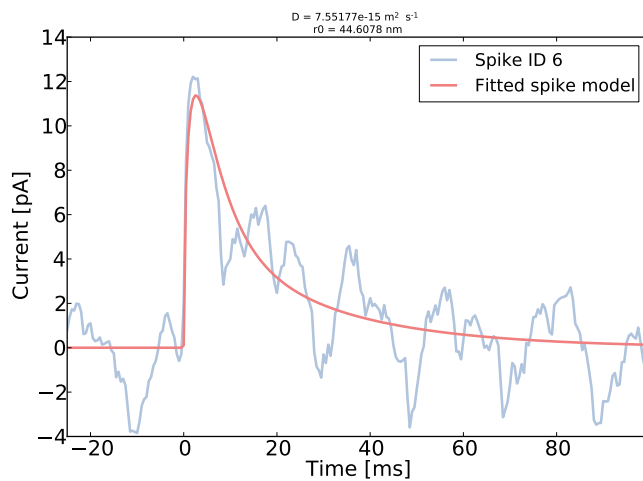
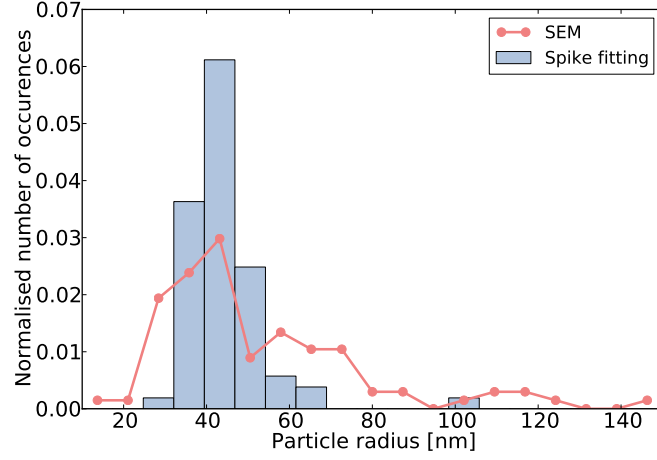


Figure 5: Examples of least-squares fits of the analytical solution for the current transients transformed according to the potentiostat's transfer function to experimental data.

a)



b)

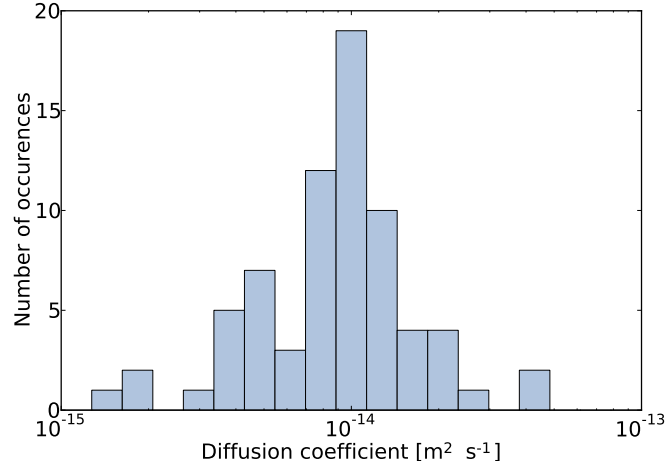


Figure 6: Comparison between previous scanning electron microscopy measurements⁷ and the distribution of fitted particle radii a) and diffusion coefficients obtained from fitting the spike model to experimental data b).

Our theoretical model considers the electrochemical doping of nanoparticles impacting on an electrode as a Fickian diffusion process of ions inside of an initially depleted spherical space. The solution of this analytical model for the resulting charge transfer at the electrode and a numerical model for the response characteristics of the analogue circuitry of the measurement equipment, which we found to exhibit first-order low-pass filter characteristics, enables the understand and prediction experimentally-observed spike shapes. A large data set of current measurements is automatically analysed by a software package that was devel-

oped for the purpose of this study and various physical parameters are extracted from the spike shapes. We determine the particle size distribution, which exhibits excellent agreement with scanning electron microscope measurements, and measure the diffusion coefficient of the tetrafluoroborate anion in ferrocene nanoparticles to about $10^{-14} \text{ m}^2 \text{ s}^{-1}$.

Supporting material

Determination of the spatiotemporal concentration profile, implementation of the boundary conditions in the solution of diffusion equation, analytical solution for the current transient, characterisation of the potentiostat, computational model of the filter response, finite-differences simulations, automated spike finding, automated spike fitting, numerical validation of the analytical solution to the current transient, discussion of the numerical accuracy of the presented model.

Acknowledgement

The research leading to these results has received partial funding from the European Research Council under the European Union’s Seventh Framework Programme (FP/2007-2013) / ERC Grand Agreement n. [320403].

References

- (1) Cheng, W.; Compton, R. G. Electrochemical Detection of Nanoparticles by Nano-Impact Methods. *TrAC-Trend. in Anal. Chem.* **2014**, *58*, 79–89.
- (2) Rees, N. V. Electrochemical Insight from Nanoparticle Collisions with Electrodes: A Mini-Review. *Electrochem. Comm.* **2014**, *43*, 83–86.

- (3) Pumera, M. Impact Electrochemistry: Measuring Individual Nanoparticles. *ACS Nano* **2014**, *8*, 7555–7558.
- (4) Batchelor-McAuley, C.; Kätelhön, E.; Barnes, E. O.; Compton, R. G.; Laborda, E.; Molina, A. Recent Advances in Voltammetry. *ChemistryOpen* **2015**, *4*, 224–260.
- (5) Zhou, Y.-G.; Rees, N. V.; Compton, R. G. The Electrochemical Detection and Characterization of Silver Nanoparticles in Aqueous Solution. *Angew. Chem. Int. Ed.* **2011**, *50*, 4219–4221.
- (6) Cheng, W.; Zhou, X.-F.; Compton, R. G. Electrochemical Sizing of Organic Nanoparticles. *Angew. Chem.* **2013**, *125*, 13218–13220.
- (7) Feng, A.; Cheng, W.; Holter, J.; Young, N.; Compton, R. G. Controlled Variable Oxidative Doping of Individual Organometallic Nanoparticles. *Chem.-Eur. J.* **2016**, *22*, 6981–6986.
- (8) Kätelhön, E.; Tanner, E. E.; Batchelor-McAuley, C.; Compton, R. G. Destructive Nano-Impacts: What Information Can Be Extracted from Spike Shapes? *Electrochim. Acta* **2016**, *199*, 297–304.
- (9) Haddou, B.; Rees, N. V.; Compton, R. G. Nanoparticle–Electrode Impacts: The Oxidation of Copper Nanoparticles Has Slow Kinetics. *Phys. Chem. Chem. Phys.* **2012**, *14*, 13612–13617.
- (10) Lin, Q.; Compton, R. G. Quantifying Adsorption on Single Alumina Particles via Impact Voltammetry and Current Transient Analysis. *J. Phys. Chem. C* **2015**, *119*, 23463–23469.
- (11) Hellberg, D.; Scholz, F.; Schubert, F.; Lovric, M.; Omanovic, D.; Hernández, V. A.; Thede, R. Kinetics of Liposome Adhesion on a Mercury Electrode. *J. Phys. Chem. B* **2005**, *109*, 14715–14726.

- (12) Li, Y.; Deng, H.; Dick, J. E.; Bard, A. J. Analyzing Benzene and Cyclohexane Emulsion Droplet Collisions on Ultramicroelectrodes. *Anal. Chem.* **2015**, *87*, 11013–11021.
- (13) Sekretaryova, A. N.; Vagin, M. Y.; Turner, A. P.; Eriksson, M. Electrocatalytic Currents from Single Enzyme Molecules. *J. Am. Chem. Soc.* **2016**, *138*, 2504–2507.
- (14) Bronstein, I. N.; Semendjajew, K. A.; Musiol, G.; Mühlig, H. *Taschenbuch der Mathematik*, 5. Auflage; Verlag Harry Deutsch, 2001.
- (15) Institute, R. P. Script: Heat Conduction in Cylindrical and Spherical Coordinates. <http://www.ewp.rpi.edu/hartford/~ernesto/S2006/CHT/Notes/ch03.pdf> accessed in June 2016.
- (16) Crank, J. *The Mathematics of Diffusion: 2nd Edition*; Clarendon Press, 1975.
- (17) Compton, R. G.; Laborda, E.; Ward, K. R. *Understanding Voltammetry: Simulation of Electrode Processes*; World Scientific, 2013.
- (18) Thomas, L. Elliptic Problems in Linear Differential Equations over a Network. *Watson Scientific Computing Laboratory Report, Columbia University, New York*. **1949**,

Graphical TOC Entry

